Available online at www.sciencedirect.com
ScienceDirect
Journal of Applied Geophysics 64 (2008) 1 – 13
JOURNAL OF APPLIED GEOPHYSICS
www.elsevier.com/locate/jappgeo

Two different approaches for georadar data processing: A case study in archaeological prospecting

Luciana Orlando [a,*], Francesco Soldovieri [b]

[a] Dipartimento di Idraulica Trasporti e Strade, La Sapienza University, Via Eudossiana, 18 Rome, Italy
[b] Istituto per il Rilevamento Elettromagnetico dell'Ambiente, Consiglio Nazionale delle Ricerche, Via Diocleziano 328, 80124 Napoli, Italy

Received 8 January 2007; accepted 12 October 2007

Abstract

This paper deals with the application of two different processing methods of the georadar data aimed at improving the results in the case of bad quality data. The georadar data are referred to two areas located in the Axum archaeological park (Ethiopia) and were acquired prior to the reinstallation of the returned Stele from Italy to the Ethiopian Government. In the area the schist formation is covered by an outcropping sandy silt formation about 6–8 m thick. The archaeological excavations, performed before the georadar data acquisition, revealed that tombs and catacombs were dug into the superficial layer. Because the complexity of the georadar data interpretation based on standard data processing, some of the collected measured data are also processed by an innovative microwave tomographic approach which permits to achieve clearer diagnostic results with respect to the classic radaristic techniques in 2D and 3D representation. We take into account the data acquired for the East stele 2 with 100 MHz antenna and in the parking area of the archaeological park with 200 MHz antenna. The data were acquired on profiles 1 m apart. Comparing the data processed with the two different approaches, we obtained an improvement of the vertical resolution and of the quality of image on time slices using the tomographic approach compared to the results obtained with the classic radar one.
© 2007 Elsevier B.V. All rights reserved.

Keywords: Georadar; Archaeology; 3D data; Spatial resolution; Microwave tomography

1. Introduction

Due to its enormous weight (150 tons), the transportation of the Axumite-age stele from Italy to Ethiopia was a real endeavour. The Stele had to be restored to its original site that was declared Heritage of Humanity by UNESCO in 1984. However, the fact there might still undetected archaeological ruins or artefacts buried under the site further complicates the restoration operations.

The Stele is the second largest in the archaeological park of Aksum and probably collapsed in the XII century. In 1937, it was brought to Italy and was set in front of the Ministry of the Colonies in Rome. In April 2005, it was returned to the Ethiopian Government.

Thus, before re-erecting the Stele, georadar data were acquired with the aim of reconstructing the features of the underground; this was needed to preserve the potentially undetected fragile archaeological structures buried near the Stele 2 site during its re-erection. In particular, it is known from archaeological investigations (Munro-Hay, 1991; Phillipson, 1991) that several tombs and catacombs are buried around the original stele site. These archaeological structures were built in part on silty–sand alluvial sediments, about 6–8 m thick and in part on Precambrian schist formation. The top of the discovered archaeological structures have their top at a depth between one meter and 3–5 m from the topographic level. However, now the exact location of the most structures and the archaeological superposition of structures are relatively unknown; in fact, in the past the area has been excavated many times and recovered with sediments by archaeological excavation and robbery. Therefore, before the reinstalling of the Stele, non invasive prospecting of the subsurface has been necessary to prevent

* Corresponding author.
E-mail addresses: luciana.orlando@uniroma1.it (L. Orlando), soldovieri.f@irea.cnr.it (F. Soldovieri).

0926-9851/$ - see front matter © 2007 Elsevier B.V. All rights reserved.
doi:10.1016/j.jappgeo.2007.10.002

damage to the any unknown archaeological structures buried underneath (Orlando, 2006).

Given the geo-archaeological setting of the area, which consists of structures built with stone and/or cavities enclosed in silty–sand sediments located above the water table, the georadar was identified as the most suitable geophysical method for the high resolution of the first meters below the topographic level. In particular, the georadar surveys were carried out mainly in the area surrounding the original site of the Stele 2.

The exploitation of georadar in archaeological applications is very common (Barone et al., 2007; Martino et al., 2006; Abbas et al., 2005; Orlando, 2005; Tallini et al., 2004; Leckebusch, 2003; Piro et al., 2002; Basile et al., 2000; Conyers and Goodman, 1997; Malagodi et al., 1996). The georadar is usually exploited in a configuration, where the receiving and transmitting antennas are separated by a small fixed offset and are moved very close to or in contact with the ground-interface and for each position a time domain trace is collected. The traces are then joined and processed in order to visualize vertical profiles; in archaeology more and more frequently the profiles are acquired one close to the other so as to perform a 3D cube data and time slices that represent sections of data at a constant depth.

When the structures are well preserved and the embedding strata are electromagnetically homogeneous the time slice allows to perform an easy interpretation of anomalies in terms of archaeological structures (Piro et al., 2002; Malagodi et al., 1996). However, in some cases the anomalies are not easily interpretable and so it is very useful to make a joint interpretation of the time slices and of the vertical profiles. In fact, when many structures are superimposed it is difficult to separate different interfaces; this arises because of the limited depth resolution due to the time-signature of the transmitting antenna. In fact, the depth resolution depends on the frequency and on the electromagnetic velocity of the probing radiation of the investigated structures; moreover thin resistive structures, depending on the thickness as function of frequency of electromagnetic signal, can originate resonance phenomena. The lateral resolution depends on antenna frequency, depth and distance of profiles, the latter can induce on the time slices a stretching of the anomalies in the normal direction of profiles (Orlando, 2005) because of the different sampling of the underground. Also, it is necessary to account the role of the losses in the investigated medium, which entails to reducing the peak antenna frequency in order to achieve a good penetration depth. Therefore, in georadar surveys the choice of the antenna frequency must be performed in order to achieve a compromise between the depth resolution and the extent in depth of the domain to be investigated.

In order to improve the depth resolution, deconvolution techniques (Yilmaz, 2001), commonly exploited for the seismic data, can be exploited; however, as the radar signal has a not zero phase and its wide band is about 1.5 octave, often bad results are achieved with the application of such techniques.

Recently, in order to improve the quality of georadar diagnostic results, microwave tomographic approaches are gaining an increasing interest (Persico and Soldovieri, 2004; Soldovieri and Persico, 2004; Cui and Chew, 2002; Meincke, 2001). Microwave tomography approaches are based on the solution of an inverse scattering problem (Soldovieri and Persico, 2004) with the aim of determining the spatial distribution of the dielectric and/or conductive characteristic of a subsurface region from scattered field data gathered at the air-soil interface. This technique permits not only to detect the target but also to accurately locate it and determine its geometrical features in terms of extent and shape.

In particular, in this paper we compare the results of a 1D microwave tomographic processing applied to the measured data collected in the Aksum Park with those achieved by the classic georadar processing.

The paper is organised as follows. In Section 2, the microwave tomographic approach is briefly described and some reconstruction results with synthetic data are presented. Section 3 is devoted presenting the geoaradar survey in Aksum and the main results processed by the classic radar technique. Then, in Section 4, we show the results obtained by the tomographic approach and compare them with the classic radar results presented in Section 2. Finally, conclusions follow.

2. The microwave tomographic approach

This Section is devoted to presenting the microwave tomographic approach exploited in the processing of the measurements.

The microwave tomography technique has become an increasingly popular interpretational tool for Ground Penetrating Radar (GPR) applications. The possibility of recasting the data processing as an inverse scattering problem (Colton and Kress 1992) can improve the interpretation of simpler "radargrams" (Daniels, 2004). Indeed it allows to obtain more focalized and clearer images of the subsurface in order to have a more objective representation of the investigated area in terms of presence, location and geometrical properties of the targets (Persico and Soldovieri, 2004; Soldovieri and Persico, 2004). In addition, the adoption of more accurate models of the electromagnetic scattering phenomenon, can help us understand crucial aspects of a specific problem at a much deeper interpretational level.

In this paper, we exploit an inverse scattering algorithm that works in the frequency domain and is able to face the problem in 1D-geometry in order to process the single traces collected by the georadar. Then, the vertical profiles are achieved by joining the tomographic reconstruction of the single traces of the same measurement line. The 3D description of the investigated area is obtained by joining the vertical profiles; finally the time slices are achieved as interpolated sections of the 3D cube at a constant depth.

In particular, the inverse scattering algorithm here considered assumes the 1D half-space geometry where one of the media is the air (where the antenna is located) and the other one is the soil where the targets are buried (see Fig. 1).

We assume both the two half-spaces as homogeneous media and the soil has been considered with conductive losses. The first medium is air and has a relative dielectric permittivity $\varepsilon_1 = 1$. The soil has a relative equivalent complex dielectric permittivity

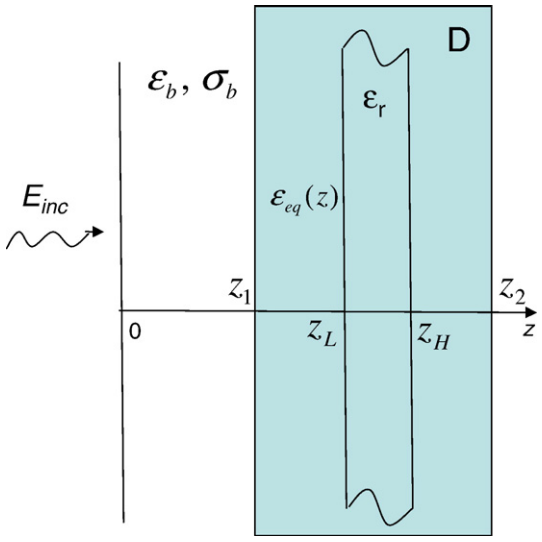

Fig. 1. Geometry of the inverse scattering problem for the 1D geometry.

$\varepsilon_{eqb} = \varepsilon_0\varepsilon_b - j\frac{\sigma_b}{2\pi f\varepsilon_0}$ where ε_b and σ_b are the relative dielectric permittivity and the conductivity of the soil and f is the work frequency. The magnetic permeability is everywhere equal to that of the free space μ_0.

We assume that an unitary plane wave, whose electric field is given by e^{-jk_0z}, being k_0 the wave-number in the air-half-space, normally impinges on the investigation domain at different frequencies in a fixed range $\Omega=[f_{\min}, f_{\max}]$. For each frequency in the band $\Omega=[f_{\min}, f_{\max}]$, the scattered field is gathered at the interface air/soil located at $z=0^-$.

The scattered field is defined as the difference between the total field and the incident field. The total field is the field reflected by the soil when also the buried target is present as well. The incident field is the field reflected by the soil only and in absence of the target and accounts only the reflection from the interface air/soil.

The problem at hand is concerned with the determination of the one-dimensional dielectric profile $\varepsilon_{eq}(z)$ in the probing domain $D=[z_1, z_2]$ embedded in the soil, starting from the knowledge of the scattered field. To solve such an inverse scattering problem is, in general, a complicated task due to ill-posedness and non-linearity (Bertero and Boccacci, 1998; Pierri et al., 2002). Ill-posedness means that the problem of the "stability" of the solution against noise and uncertainties must be accounted for; this entails the adoption of regularization schemes (Bertero and Boccacci 1998) that allow to achieve an approximate version of the unknown represented by a finite number of parameters. The non-linearity implies that, due to the problem of possible false solutions (local minima) within the solution algorithm, the diagnostic results might be very different from the "true situation" also in the "ideal case" of noiseless data.

The above mentioned difficulties can be overcome by adopting a simplified model of the electromagnetic scattering; in this paper we deal with an inversion approach that exploits a linear model of the electromagnetic scattering based on the Born Approximation (BA) (Persico and Soldovieri, 2004; Soldovieri and Persico, 2004; Cui and Chew, 2002; Meincke, 2001). The adoption of Born Approximation mainly consists in neglecting the mutual interactions between the buried targets and between the targets and the air/soil interface. The adoption of BA allows the following advantages: the problem of the false solutions is avoided; the computational burden is reduced and thus it is possible to investigate large domains, in terms of probing wavelength, in a reasonable computational time. In addition, the

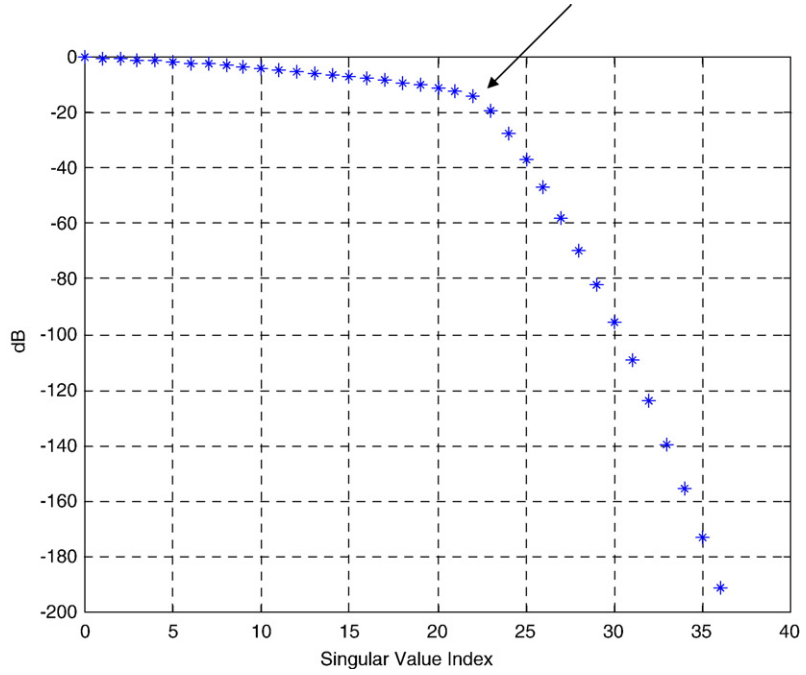

Fig. 2. Behavior of the singular value for the synthetic data. A knee (indicated by the arrow) appears around the singular value index equal to 21.

simpler linear model allows analyzing the reconstruction capabilities of the solution algorithm in terms of the spatial variations of the unknown that can be retrieved and ultimately of the achievable resolution limits as it is shown below.

Under the BA, a linear integral relationship between the contrast function (the unknown of the problem) and the scattered field (the datum of the problem) is achieved as

$$E_s(f) = k_s^2 \int_D G_e(z',f) E_{\text{inc}}(z',f) \chi(z') dz' \quad f \in \Omega \tag{1}$$

where the actual unknown of the problem is the contrast function defined by

$$\chi(z') = \frac{\varepsilon_{\text{eq}}(z') - \varepsilon_{\text{eqb}}}{\varepsilon_{\text{eqb}}} \tag{2}$$

and

$$\varepsilon_{\text{eq}}(z') = \varepsilon_0 \varepsilon_D(z') - j\frac{\sigma_D(z')}{2\pi f \varepsilon_0} \tag{3}$$

$\varepsilon_D(z')$ and $\sigma_D(z')$ being the relative dielectric permittivity and the conductivity of the unknown layers in the investigation domain D. The "contrast" function is the relative difference between the unknown dielectric profile and the electromagnetic properties of the background medium. By its definition, $\chi(z')$ is different from zero only within the investigation domain $D=[z_1, z_2]$. $k_s = 2\pi f \sqrt{\varepsilon_0 \varepsilon_{eqb} \mu_0}$ is the wave number of the soil. $E_{inc}(z', f)$ is the incident field in the investigation domain, i.e., the field present in the investigation domain D when layers (targets) are not present; it is given by:

$$E_{inc}(z',f) = T_{21} \exp(-jk_s z') \tag{4}$$

where $T_{21} = \frac{2k_0}{k_0 + k_s}$ denotes the transmission coefficient from the air to the soil half space.

G_e is the external Green's function of the background and represents the electric field radiated at the interface air/soil by a 1D impulsive source located at depth z'. Its expression is:

$$G_e(z',f) = -j\frac{T_{12}}{2k_s} \exp(-jk_s z') \tag{5}$$

where $T_{12} = \frac{2k_s}{k_s + k_0}$ denotes the transmission coefficient from the soil to the air half space.

By substituting the expressions of the Green's function and of the incident field in Eq. (1), we obtain the integral expression of the scattered field:

$$E_{sl}(f) = F(f) \int_D \chi(z') \exp(-j2k_s z') dz' \quad f \in \Omega \tag{6}$$

where $F(f) = -jT_{12}T_{21}k_s/2$ is the quantity outside of the integral that depends only on the frequency.

Therefore, the problem at hand is cast as the inversion of the linear integral equation in (6); in order to find a stable solution of the inversion of the integral relation, a regularized inversion scheme is used at the cost of renouncing to an extremely detailed resolution in the reconstruction (Bertero and Boccacci 1998). In this paper, the stability of the solution is imposed by means of a Truncated Singular Value Decomposition (TSVD) (Bertero and Boccacci 1998) of the matrix accounting for relationship (6). The matrix is achieved by the discretization of relation (6) thanks to the method of the moments where the unknown contrast function is discretized by rectangular pulse functions and the scattered field is collected in the work frequency band $\Omega=[f_{\min}, f_{\max}]$ at an uniform step.

In particular, the Truncated SVD solution is approximated as:

$$\chi = \sum_{n=0}^{N} \frac{1}{\sigma_n} < E_s, v_n > u_n \tag{7}$$

where $\langle \cdot, \cdot \rangle$ denotes the scalar product with respect to the frequency, the set $\{\sigma_n\}_{n=0}^{\infty}$ denotes the singular values ordered in a non increasing sequence, u_n and v_n are the basis functions within the space of the "visible" unknowns (i.e., the functions that can be retrieved by the noise-free data) and the space of the noise-free data for the linear integral operator (relationship) defined in Eq. (6), respectively (Bertero and Boccacci 1998). In general, the regularization is performed by choosing a truncation index N in the summation (7) according to the available signal-to-noise ratio, i.e., it consists in summing up only those terms in (7) corresponding to singular values for which σ_n/σ_0 is larger than the signal-to-noise ratio.

The SVD allows also a thorough analysis of the reconstruction capabilities of the solution algorithm in dependence of the dielectric permittivity of the host medium and of the work frequency band. It is worth noting that the problem in Eq. (6) very similar, apart the factor $F(f)$ outside the integral, to the inversion of a Fourier Transform with limited data. For such a problem an analytical determination of the singular system is possible in the case of lossless soil (Pierri et al., 2002) and this gives guidelines in theoretically providing an estimate of the number of singular values to be retained in TSVD as

$$N = \frac{(z_2 - z_1)\sqrt{\varepsilon_b}}{c_0 \pi} 2\pi (f_{\max} - f_{\min}) = \frac{2(z_2 - z_1)\sqrt{\varepsilon_b}}{c_0} (f_{\max} - f_{\min}) \tag{8}$$

where $c_0 = 1/\sqrt{\varepsilon_0 \mu_0}$ is the electromagnetic velocity in air.

In fact, for the case at hand, the singular values exhibit "step-like" behavior, and this leads to the choice of an "optimal value of N" weakly dependent on the noise level on data. As matter of fact, it is sufficient to choose as N index the one corresponding to the *knee* of the curve of the singular values. In fact, even a significant increase in the signal-to-noise ratio would not lead to a meaningful increase of the singular values to be retained in TSVD expansion (7), due to the fast exponential decay of the singular values after the knee.

The above consideration is made clear by considering a test case where a background scenario represented by a homogeneous half space with relative dielectric permittivity $\varepsilon_b=10$

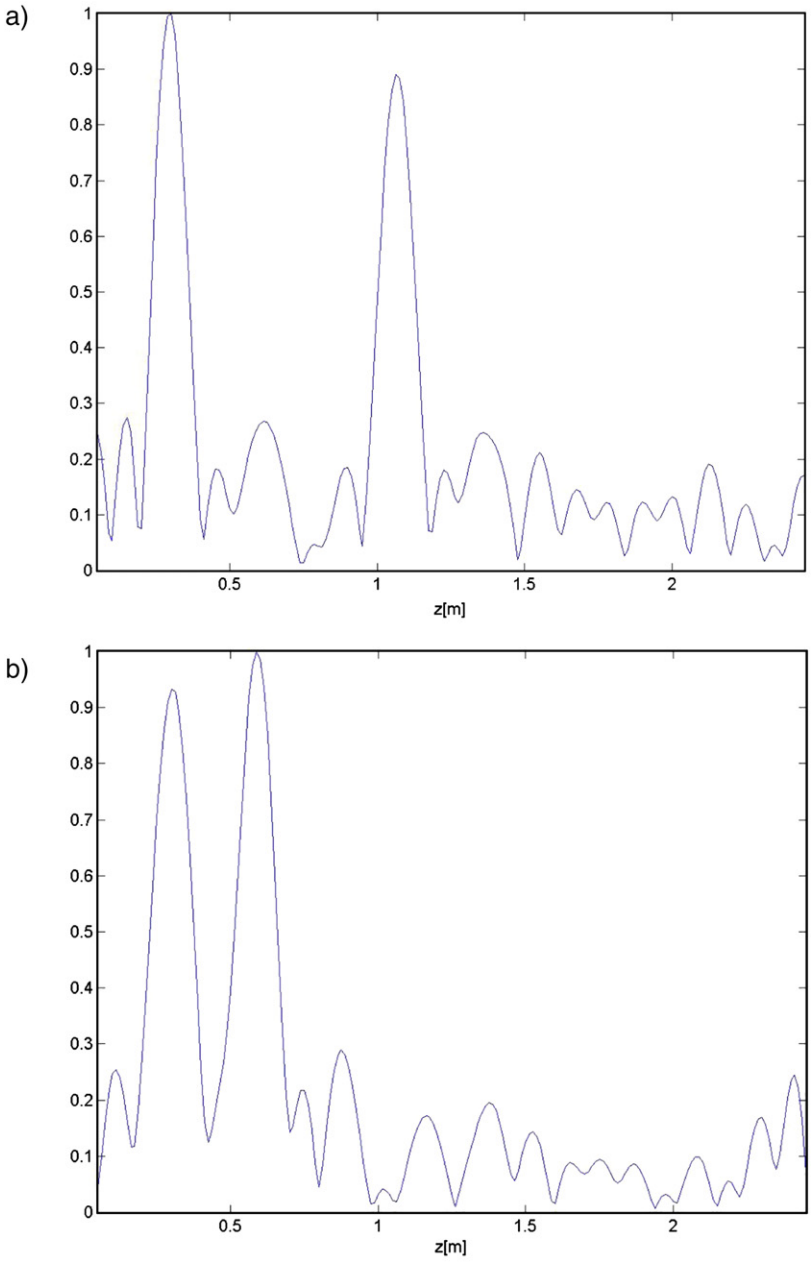

Fig. 3. Tomographic reconstruction of a slab with synthetic data. Fig. 3a and b depict the modulus of the retrieved contrast function normalized with respect to its maximum.

and an investigation domain D=[0,2.5]m are assumed. The work frequency band ranges from 100 to 500 MHz with a step of 10 MHz. Fig. 2 depicts the behavior of the singular values; as expected the singular values behavior is step like with an asymptotic exponential decay. It is worth noting that for the this case, the estimate in Eq. (8) provides N=21 that is consistent with the singular values behavior presented in Fig. 2, where the knee is about the index equal to 21.

The estimate (8) also makes it possible to give an estimate of the resolution distance, according to the Rayleigh's criterion, as (Pierri et al., 2002)

$$R = \frac{c_0}{2(f_{\max} - f_{\min})\sqrt{\varepsilon_b}} \tag{9}$$

It is worth noting that the estimate in (9) agrees with the well known rule used in radar approaches where the range resolution is a quantity inversely proportional to the bandwidth.

Let us turn now to present two numerical inversion results that consider the background scenario described above. Noisy data are considered with a signal to noise ratio equal to 20 dB; accordingly for the computation of the solution we retain in the TSVD summation of Eq. (5) the terms corresponding to the singular values 0.1 times larger than the maximum singular value.

The first reconstruction refers to a homogeneous target with relative dielectric permittivity ε_r=36 and with a thickness of 0.4 m (Fig. 3a). The first interface of the target is located at 0.3 m; thus the locations of the two interfaces are z_L=0.3 m z_H=0.7 m. The modulus of the contrast function reconstructed through the

TSVD is depicted in Fig. 3a. The location of the reconstructed peak corresponding to the second interface is at about 1.1 m. The difference between the position $\hat{z}$ of the position of the reconstructed peak and of the actual interface's location z_H can be easily justified. The difference arises since the velocity assumed in the inversion model and given by $v_b = c_0/\sqrt{\varepsilon_b}$ is different from the actual electromagnetic velocity in the slab given by $v_r = c_0/\sqrt{\varepsilon_r}$. In particular, when the relative dielectric permittivity of the slab is larger than the one of the host medium, i.e. $\varepsilon_r > \varepsilon_b$, the propagation velocity of the electromagnetic wave assumed in the model $v_b = c_0/\sqrt{\varepsilon_b}$ is larger than the actual velocity $v_r = c_0/\sqrt{\varepsilon_r}$; this leads to a delocalization in depth of the second interface of the defect $\hat{z} > \hat{z}_H$. It is possible to determine the correct location of the second interface by exploiting the relation $\hat{z} = z_H + \sqrt{\varepsilon_r/\varepsilon_b - 1}(z_H - z_L)$ where the knowledge of ε_r is assumed a priori; this relation allows to correctly determining the location z_H=0.7.

The reconstruction result allows us to state that despite of a not negligible model error, the inversion of Eq. (6) allows localizing the fast discontinuities of the contrast profile that correspond to the interfaces of the layer (Pierri et al., 2002, Persico and Soldovieri, 2004; Soldovieri and Persico, 2004). This kind of reconstruction result is consistent with the fact that the inversion of Eq. (6) permits to achieve a band-pass filtered version of the contrast function; this entails that in the reconstruction the fast spatial variation of the unknown are privileged. Accordingly, the reconstruction algorithm is able to detect and localize the two interfaces of the penetrable target.

The second numerical results is concerned with a layer that has a relative dielectric permittivity ε_r=5. The modulus of the contrast function via TSVD is depicted in Fig. 3b. Now, we have $\varepsilon_r < \varepsilon_b$; in this case the difference in the velocity of the electromagnetic wave in the slab and in the host medium entails a reconstructed peak which "anticipates" the actual location of the second interface, i.e., $\hat{z} < z_H$. It is still possible to determine the correct location of the second interface by exploiting the relation $\hat{z} = z_H + \left(\sqrt{\varepsilon_r/\varepsilon_b - 1}\right)(z_H - z_L)$ where the knowledge of ε_r is assumed a priori.

For both the cases, the relation of Eq. (9) provides an estimate of the resolution distance R equal to 0.12 m. Thus, for the two numerical reconstructions we have the peaks (corresponding to the interfaces) spaced at distance (0.8 m and 0.28 m for the first and second case, respectively) greater than the resolution distance R.

We stress that the inversion algorithm is exploited in this paper to process data collected by a commercial time domain georadar (see the section below), therefore, the actual measurements collected by the georadar are in time-domain and accounts also for the reflection by the air/soil interface and of the "desired response" from the buried targets. Therefore, the problem of extracting the scattered field (response only of the buried targets) from the total one (response of the air/soil interface plus response of the buried targets) arises. In this paper, this extraction is performed by time gating the measurements collected by the georadar. Then, these gated measurements undergo to a Fourier Transform to achieve frequency data suitable for the inversion code.

Finally, we roughly justify the adoption of a simple 1D inversion algorithm in the realistic cases presented below. First of all, we recall that the electromagnetic field radiated by the antenna can be given under a spectral representation (Soldovieri et al., 2005); therefore, the radiated field (i.e., the incident field in our inversion) can be "physically interpreted" as the superposition of plane waves of different propagation directions. Differently in our inversion scheme we consider as incident field a plane wave with normal incidence (i.e., incidence direction along the z-axis). Therefore, an approximation arises in the evaluation of the incident field. However, we can state that this approximation is roughly valid since the reflected field in the wave directions near normal incidence provides in most cases the biggest contribution to reflected energy for small-offset antenna configurations.

3. Georadar prospecting, processing and radargram analyses

The data were collected using the instrument PulseEkko100 of Sensor & Software Corporation equipped with a 100 MHz antenna and the IDS Instrument equipped with 200 MHz antenna. The goal of the survey was to carry out a detailed reconstruction of the underground structures present, so that a distance between the profiles of 1 m was chosen. Also, profiles in both x and y directions (Fig. 4) were performed in order to avoid any ambiguity due to the direction of profiles with respect to the features of structures.

The data were acquired in continuous mode in a time window of 500 ns, with a sampling rate of 0.8 ns for the 100 MHz antenna. The time window was selected to investigate the maximum possible depth in dependence on the antenna frequency bandwidth and the ground attenuation of sediments. The antenna position along the profile was obtained thanks to markers located at an uniform step of 2 meters. For the 200 MHz antenna, the sampling rate of 0.2 ns and a time window of 200 ns were adopted; the scan positions were controlled by an odometer.

CMP data were gathered with a transmitter-receiver offset increment of 0.1 m with the PulseEkko instrument. The root-mean-square wave velocity of about 0.085–0.09 m/ns was calculated from CMP (Common Mid Point) and diffraction hyperbola. The velocity of 0.09 m/ns was used for the time/meter conversion in the diagnostic results. A theoretical vertical resolution of 0.25–0.35 m was obtained for this electromagnetic velocity and for a pulse frequency of 120–150 MHz.

The classic georadar data processing consisted in time setting, time pass-band filter, mix traces and exponential gain. Since the spatial step along the profiles acquired with PulseEkko Instrument was not constant, these profiles were spatially re-sampled prior the 3D representation is performed (Conyers and Goodman, 1997, Malagodi et al., 1996, Whiting et al., 2000).

In this paper we will show the results for the two grey areas of Fig. 4: the first one is located at the right of Stele 2 and was investigated with 100 MHz antenna and the second is located in the parking area of the archaeological site and was investigated

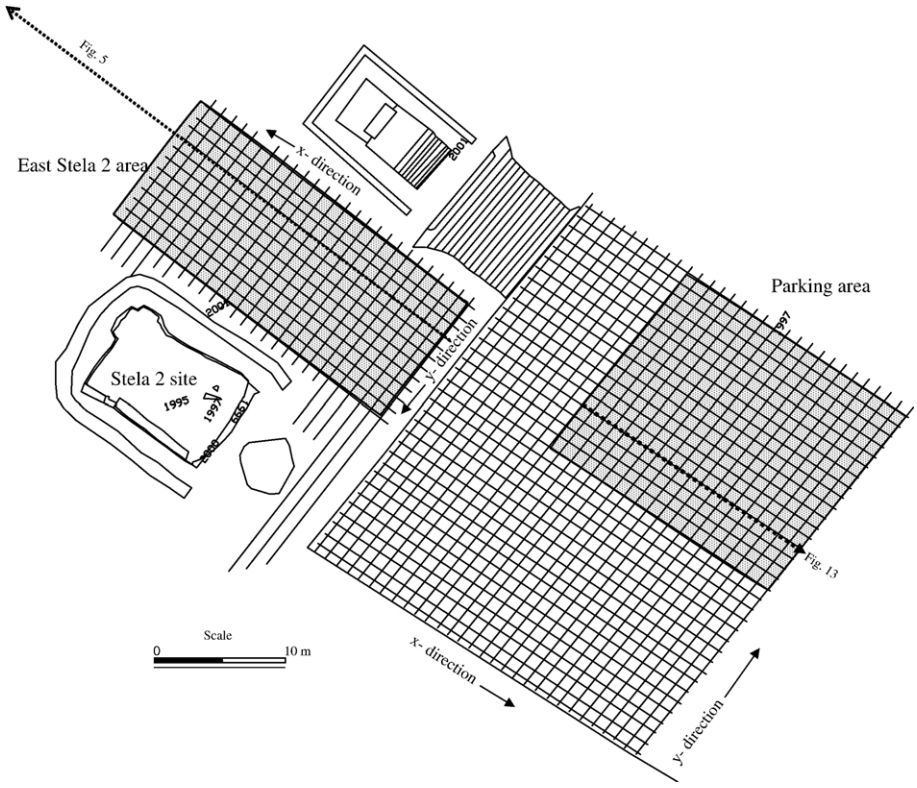

Fig. 4. Location of georadar profiles. The grey areas were discussed. The dots lines are the location of profiles shown in the Figs. 5 and 13.

with the 200 MHz antenna. In the both area we analyse only the profiles acquired in x direction.

The data will be analysed with the objective of highlighting the differences of information that can be obtained via the two different approaches, i.e., microwave tomography and usual georadar data processing, and not with the main aim of interpreting all the archaeological structures buried in the area. Therefore, let us turn now to show some of the main results of the usual processing for these two areas; the results will be compared with those achieved by the microwave tomograpic approach described in Section 2.

In the East Stele 2 area, the georadar survey shows a useful signal up to 40–60 ns (2–3 m) of the subsurface. Below the profiles are shown for lag-time windows depending on the

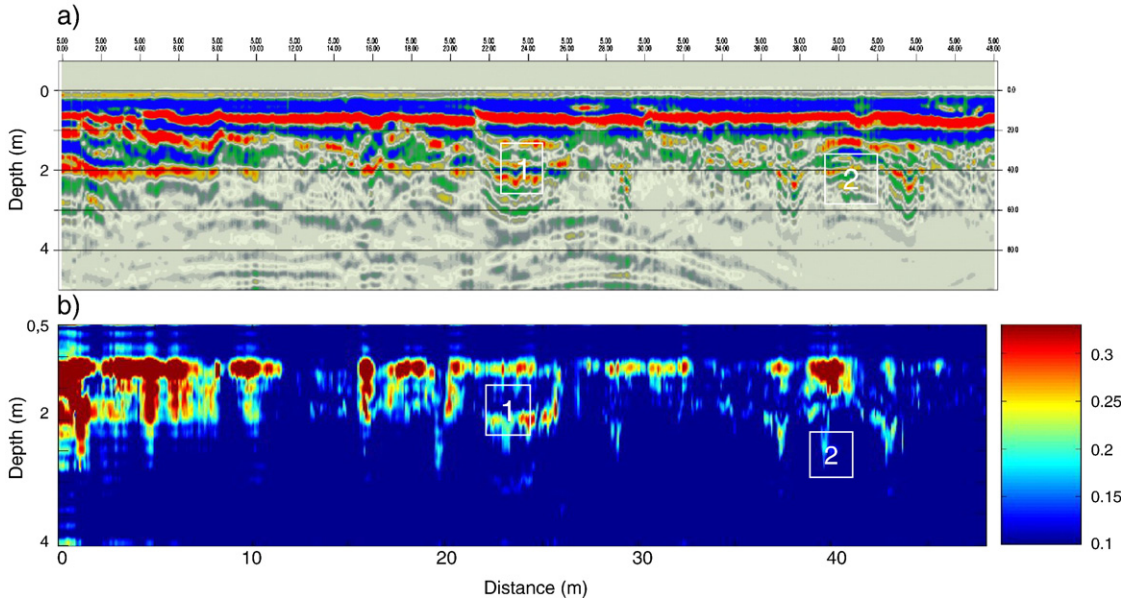

Fig. 5. Vertical georadar profile: a) Amplitude of data achieved via the classic GPR processing approach; b) Normalized amplitude with respect to its maximum of the contrast function retrieved by the microwave tomographic approach. For the location of the vertical profile see Fig. 4. The numbers indicate the zones where different depth resolution is obtained with the two different approaches.

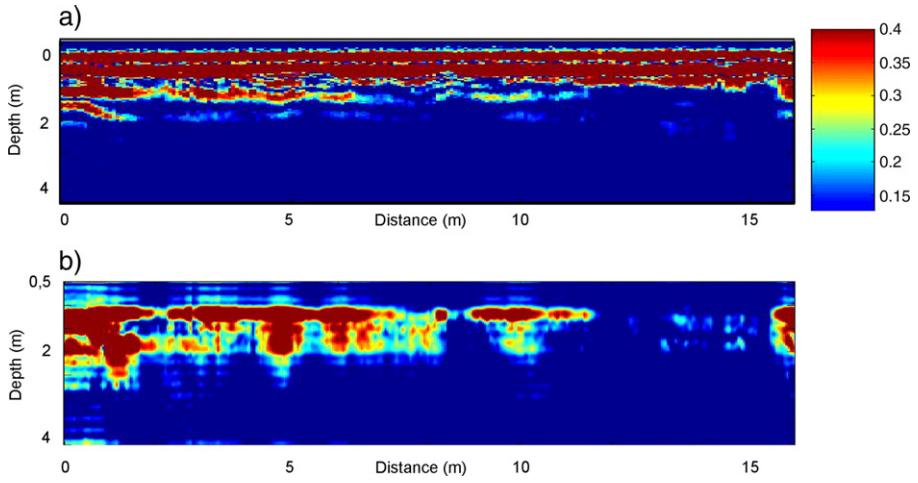

Fig. 6. Vertical georadar profile: zoom of the lag 0–16 m of profile of Fig. 5. a) Absolute amplitude normalized with respect to its maximum achieved via the classic GPR processing approach; b) Normalized amplitude with respect to its maximum of the contrast function retrieved by the microwave tomographic approach.

penetration of signal. The analyses of profiles show a very complex setting of the underground characterized by the presence of materials, structures, slabs and filled cavities.

The data interpretation, even if performed by jointly exploiting vertical profiles, time slices and measurements acquired in both perpendicular directions, was a difficult task and often it was not possible to discriminate the anomalies due to archaeological features from the noise effect.

The main anomalies were detected thanks to the exploitation of profiles acquired in *x*- and *y*- direction, but only in few cases it was possible to correlate anomalies with the archaeological structures outlined in the images collected during previous surveys in the park (Munro-Huy, 1991; Phillipson, 1991).

Let us turn now to show some results achieved by the usual radar processing; in particular we present in the figures below the modulus of the radargram.

In Fig. 5a we show the processed radargram for a vertical profile with 628 spatial points equally spaced on a 48 m wide domain and on a 100 ns time window. The profile was collected with a 100 MHz antenna at a distance of about 8 m from Stele 2 (Fig. 4).

Figs. 6a–8a give a zoom of the vertical profile of Fig. 5 over three regions 16 m wide. In particular, Figs. 6a–8a depict the modulus of the processed radargram that is normalized with respect to its maximum. The vertical profile shows anomalies which are difficult to be interpreted since the structures are not well preserved and more structures are superimposed. For example, it is very difficult to detect the upper and bottom boundaries of the structures 1 and 2 in Figs. 5, 7 and 8 because of the limited depth resolution and of the oscillating behavior of the radar signal.

The same problem arises if we analyse the time slices of the 3D representation. Such a 3D representation is achieved by joining 10 profiles 32 m long, spaced from each other by 1 m and collected with 100 MHz antenna in East Stela 2 area. The profiles consist in 480 equally spaced traces and each single trace is made of samples spaced 0.8 ns. Figs. 9–12 a depict the time slices at 0.5, 0.75, 1.1 and 1.5 m where the

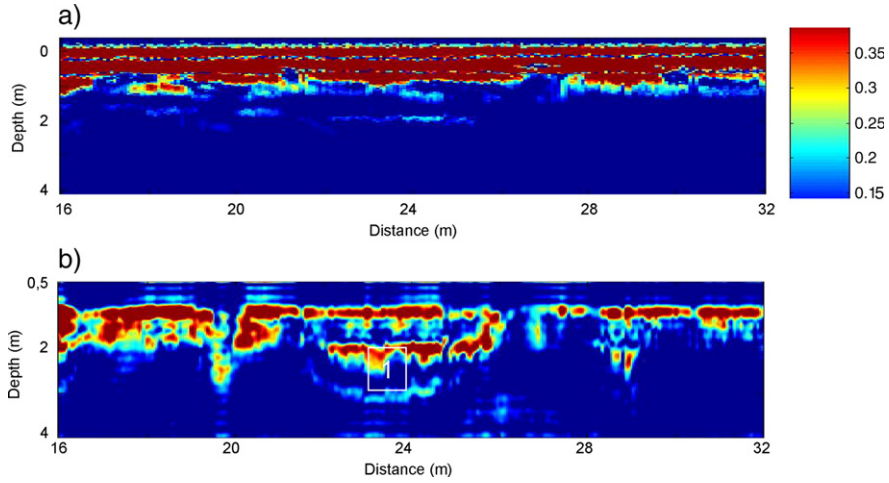

Fig. 7. Vertical georadar profile: zoom of lag 16- 32 m of profile of Fig. 5. a) Absolute amplitude normalized with respect to its maximum achieved via the classic GPR processing approach; b) Normalized amplitude with respect to its maximum of the contrast function retrieved by the microwave tomographic approach. Label 1 denotes zone where different spatial resolution is achieved by the microwave tomographic approach.

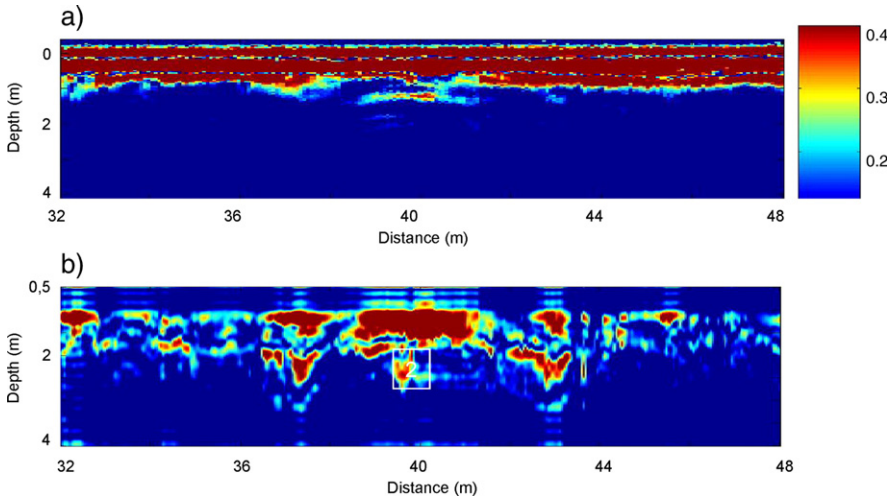

Fig. 8. Vertical georadar profile: zoom of the lag 32–48 m of profile of Fig. 5. a) Absolute amplitude normalized with respect to its maximum achieved via the classic GPR processing approach; b) Normalized amplitude with respect to its maximum of the contrast function retrieved by the microwave tomographic approach. Label 2 denotes zone where different spatial resolution is achieved by the microwave tomographic approach.

absolute amplitude of the signal normalized with respect to its maximum is shown. The anomalies appear to be very scattered and little organized and it is very difficult to assess from their geometries. Only the slice at 1.1 m (Fig. 11a) seems to have detected a circular shaped anomaly (labelled with 1 in the figure) which could be correlated to a structure.

We show also the results concerned with a different area located in the parking area at front of the archaeological park (Fig. 4) in this area we consider 17 profiles about 20 m long and spaced from each other at 1 m. The profiles are collected with the 200 MHz antenna and consist in 1040 equally spaced traces by 0.02 m. Each single trace is made of 470 time samples with a step of 0.0104 ns for an overall time-range of about 49 ns.

In this area the radar has investigated the depth of about 1.5 m (corresponding to a time widow of about 30 ns) and data interpretation allows to identify several anomalies related to the utilities of a fountain and waterworks of the park built in the sixties and now buried. In particular, we investigate an area where the rest of a buried fountain structure is present.

In Fig. 13, a vertical profile (for location see Fig. 4) crossing the modern fountain detects the edges (labelled with 1 in figure) and the bottom of the fountain. The figure is shown for a time windows of 28 ns.

As already said, 3D representation of the area is achieved by joining 17 profiles 20 m long, spaced from each other at 1 m allowed to perform the interpretation on time slices as well. The

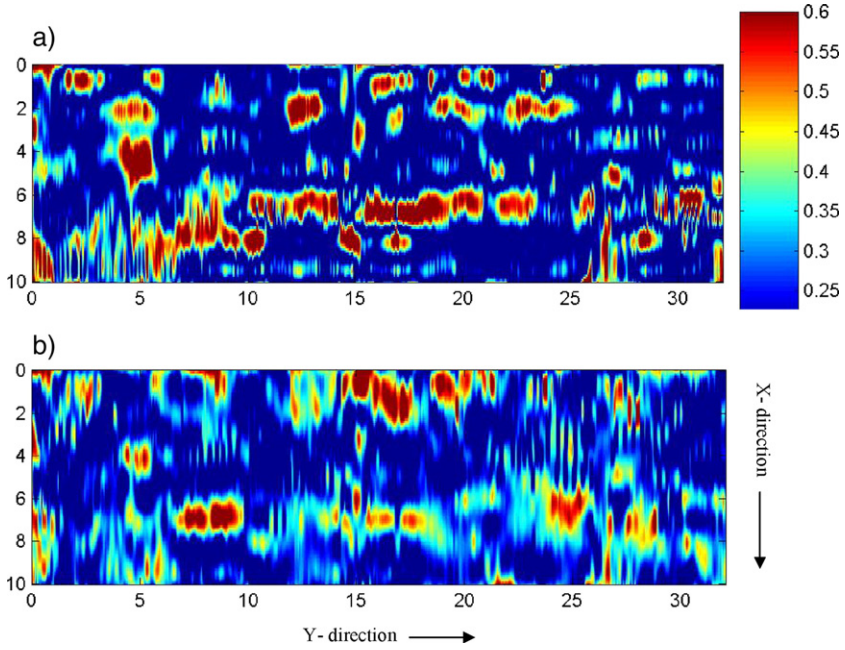

Fig. 9. Time slices at 0.5 m: a) Absolute amplitude normalized with respect to its maximum achieved via the classic GPR processing approach; b) Normalized amplitude with respect to its maximum of the contrast function retrieved by the microwave tomographic approach.

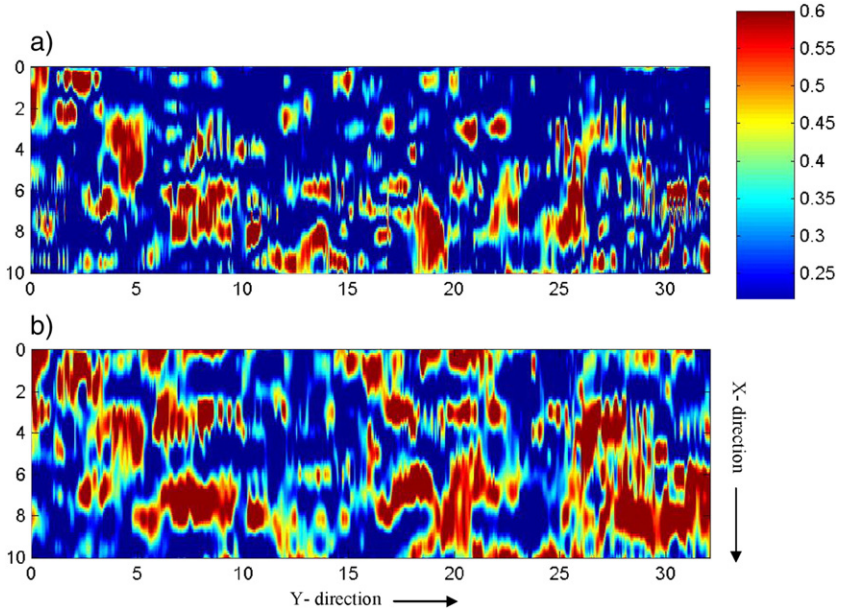

Fig. 10. Time slices at 0.75 m: a) Absolute amplitude normalized with respect to its maximum achieved via the classic GPR processing approach; b) Normalized amplitude with respect to its maximum of the contrast function retrieved by the microwave tomographic approach.

time slices at 0.25 and 0.40 m are shown in Figs. 14a and 15a, respectively. They show an anomaly with an ellipsoidal shape that was attributed to the remains of the buried modern fountain. The non regular sampling of the underground given by an over-sampling along the profiles (antenna movement direction) and the under-sampling along the direction normal to the profiles given the stretching effect on the image of time slices.

In both the considered areas, the anomalies are not clear enough to be interpreted and often the low vertical resolution has not allowed to properly outlining in a right way the boundaries of the anomalies.

In order to improve the quality of the results also in terms of depth resolution a microwave tomographic approach was applied to the data.

4. The results of the microwave tomographic approach.

This Section is devoted to presenting the results achieved via the tomographic approach and comparing them with the results of the classic radar processing approach in the two areas already described in the section above: East Stele 2 and parking area of the archaeological site (Fig. 4).

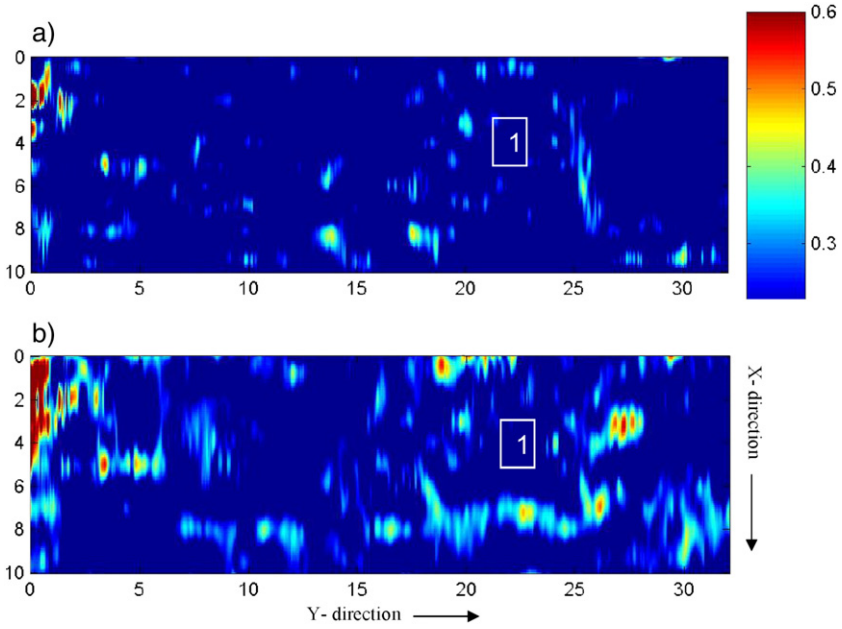

Fig. 11. Time slices at 1.1 m: a) Absolute amplitude normalized with respect to its maximum achieved via the classic GPR processing approach; b) Normalized amplitude with respect to its maximum of the contrast function retrieved by the microwave tomographic approach.

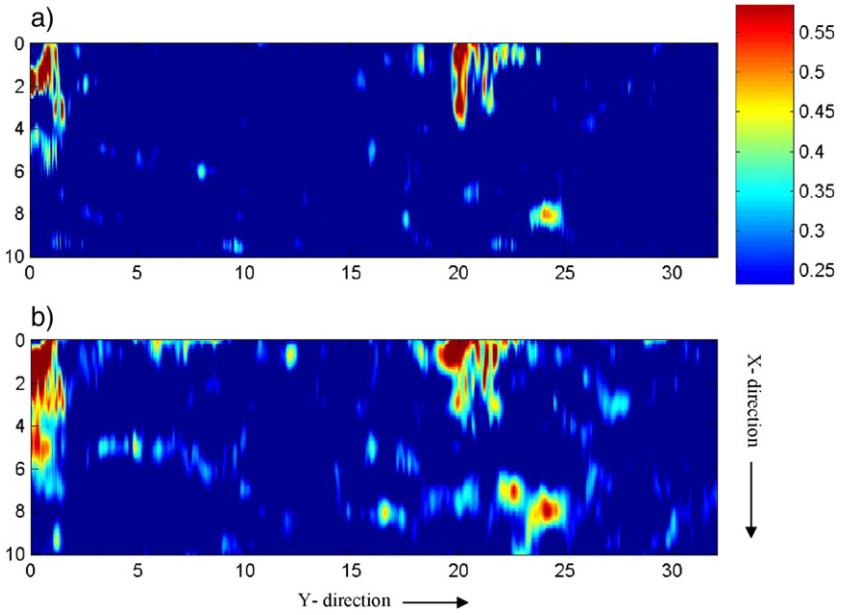

Fig. 12. Time slices at 1.5 m: a) Absolute amplitude normalized with respect to its maximum achieved via the classic GPR processing approach; b) Normalized amplitude with respect to its maximum of the contrast function retrieved by the microwave tomographic approach.

The first result concerns the East Stele 2 area where a 48 m long profile, already described in Figs. 5–8a, was collected by the 100 MHz antenna. It is made of 628 uniformly spaced traces and each single trace is sampled with a step of 0.8 ns.

The time-zero (corresponding to the air/soil interface) was fixed at the 10th time sample and a gating procedure was exploited for the first 24 ns. The gated time-domain data were then Fourier transformed in order to achieve the data in frequency domain that was suitable for the inversion scheme. For the 1D inversion we exploited a work frequency band ranging for 50 MHz to 245 MHz with a step of 3.9 MHz (51 frequency points). The investigation domain is assumed from 0.5 to 4 m of depth and the contrast function is discretised within the investigation domain by 351 rectangular pulse functions. According to the velocity analyses, the relative dielectric permittivity of the soil is assumed equal to 10.

The vertical profile is finally achieved by superposing the 1D single trace tomographic reconstructions and then by interpolating along the horizontal axis (air/soil interface) from the 628 measurement points to 2*628 points (Fig. 5 b).

The microwave tomographic result shows a better vertical and lateral resolution with respect to the georadar profile of

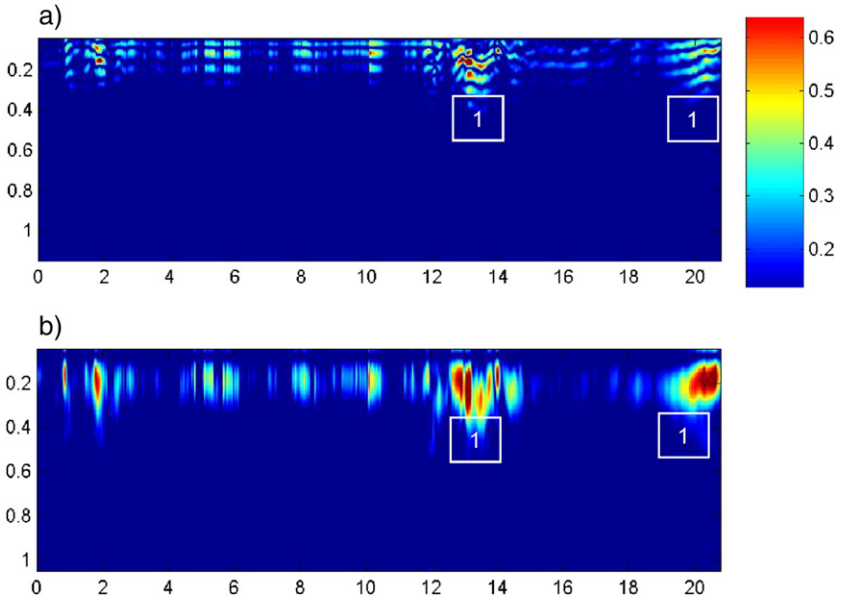

Fig. 13. Vertical profile: a) Absolute amplitude normalized with respect to its maximum achieved via the classic GPR processing approach; b) Normalized amplitude with respect to its maximum of the contrast function retrieved by the microwave tomographic approach. For location see Fig. 4.

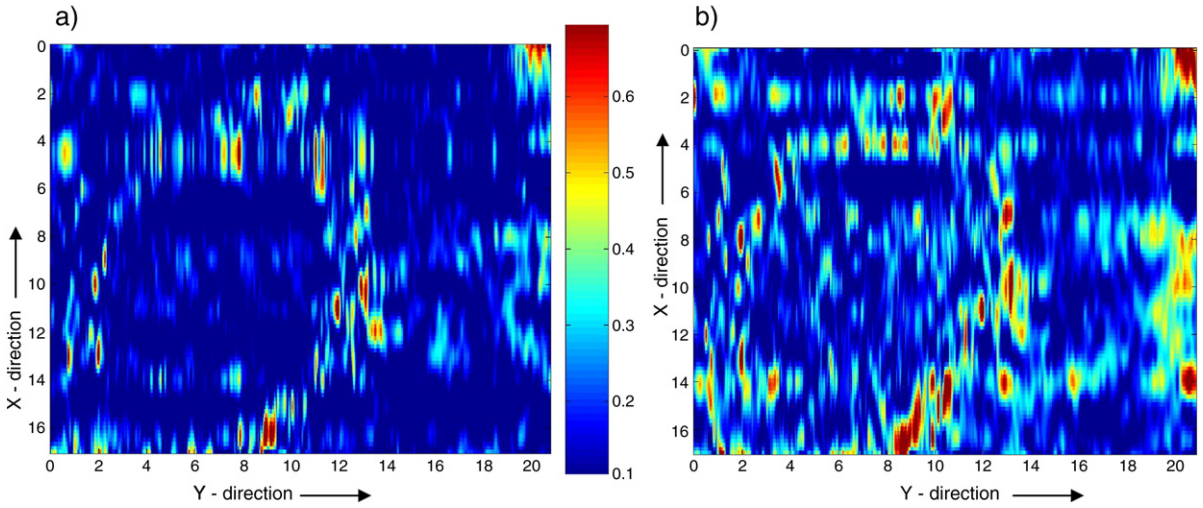

Fig. 14. Time slices at 0.25 m: a) Absolute amplitude normalized with respect to its maximum achieved via the classic GPR processing approach; b) Normalized amplitude with respect to its maximum of the contrast function retrieved by the microwave tomographic approach.

Fig. 5 a: the superficial reflector appears laterally discontinuous and the upper and bottom boundaries of anomalies 1 and 2 are clearly delineated. The air wave is removed.

Figs. 6–8b depict the tomographic reconstruction of the zoom of Fig. 5 a, reported in Figs. 6–8a in order to better point out the differences compared to the classic geoardar data processing. All the figures show an improving in the vertical resolution as clearly shown by the anomalies 1 and 2 of Figs. 7 and 8.

Let us turn now to present the tomographic reconstruction for the all 10 profiles 32 m long acquired by the 100 MHz antenna at East Stele 2. All profiles were processed in the same way of the profile described before; the reconstructions are then joined to achieve the 3D cube of the surveyed area. Fig. 9–12b depicts the modulus of the reconstructed function normalized with respect to its maximum over the time slice at 0.5, 0.75, 1.1 and 1.5 m, respectively. We observe a similarity between the results of the two approaches. However, the result achieved by the tomographic approach gives a more detailed representation of the anomalies; this behaviour is more evident on the slice at 1.1 m where the circular anomaly appears to be better depicted in Fig. 11 b. The tomographic approach reduces slightly the stretching of images due to the non regular sampling of the underground.

The processing described above was applied to the data acquired in the second area, i.e., the parking area (Fig. 4). A profile acquired on the fountain and processed with the tomographic approach is shown in Fig. 13 b. The tomographic approach allows to erase the oscillatory behaviour of the signal and thus to better point out the rest of the fountain structure buried in the area as it is visible comparing this results with that obtained with the classic GPR data processing (Fig. 13 a).

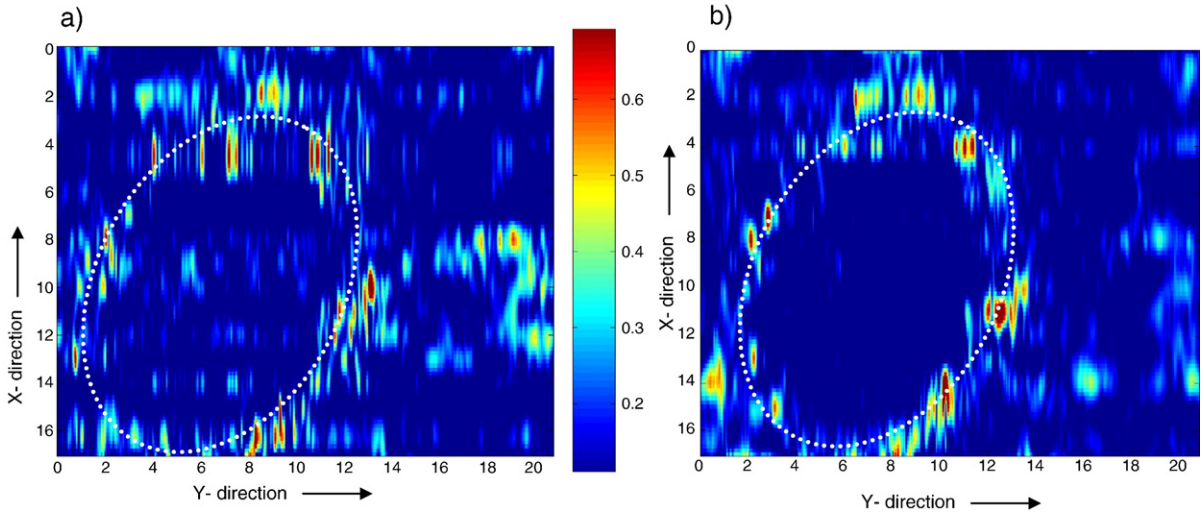

Fig. 15. Time slices at 0.4 m: a) Absolute amplitude normalized with respect to its maximum achieved via the classic GPR processing approach; b) Normalized amplitude with respect to its maximum of the contrast function retrieved by the microwave tomographic approach.

Finally, we applied the microwave tomographic approach to whole data acquired in this area. For this area (and hence also for the already shown vertical profile of Fig. 13), in 1D inversion we exploit a work frequency band ranging for 50 MHz to 350 MHz with a step of 6 MHz (51 frequency points). The investigation domain is assumed from 0.05 to 1 m of depth and the contrast function is discretised within the investigation domain by 201 rectangular pulse functions. According to the velocity analyses, the relative dielectric permittivity of the soil is assumed equal to 10. The reconstructed slices at a constant depth of 0.25 m and 0.40 m are shown in Figs. 14 b and 15 b. The comparison between the tomographic result and the classic GPR data processing shows how the microwave tomography provides an improvement of signal noise ratio, a reduction of image stretch and a more detailed description of the investigated zone mainly for the slice at depth of 0.40 m (Fig. 15).

5. Conclusions

Georadar prospecting was used to investigate the first 1.5–2.5 m of the underground close to the original site of the stele 2 and the parking area of the archaeological site. The georadar detected several anomalies same of which were associated to walls, cavities and shafts while others were difficult to be interpreted, even if the interpretation was performed on vertical and horizontal profiles and using profiles acquired at 1 m apart from each other in *x*- and *y*- direction. At first the data interpretation was obtained through the joint interpretation of vertical profiles and 3D data cube. To test the quality of results in term of vertical resolution, the data were processed and compared according two different approaches: the radar and tomographic one. The latter is an innovative processing algorithm based on microwave tomography. This approach is based on a more refined model of the electromagnetic scattering; it casts the problem as a linear inverse scattering one that is regularized by the SVD tool. The results were compared on vertical profiles and time slices as well. The comparison has shown an improvement of the vertical resolution and a better delineation of the shape of anomalies when the tomographic approach was used. In fact, for the East stele 2 area the anomaly at depth of 1.1 m is better delineated and in the parking area the buried structure of a modern fountain is cleaner compared to the results performed via the radar approach.

Acknowledgments

The research is under the sponsorship of UNESCO. We thank Prof. Claudio Margottini for his help in the data acquisition and Dr. Giuseppina Nuzzo for her help in revising the English language.

References

Abbas, A.M., Kamei, H., Helal, A., Atya, M.A., Shaaban, F.A., 2005. Contribution of geophysics to outlining the foundation structure of the Islamic Museum, Cairo, Egypt. Archaeological Prospection 12, 167–176.

Barone, P.M., Graziano, F., Pettinelli, E., Ginanni Corradini, R., 2007. Ground-penetrating radar investigations into the construction techniques of the Concordia Temple (Agrigento, Sicily, Italy). Archaeological Prospection, Published Online: 8 Jan 2007, pp. 47–59.

Basile, V., Carrozzo, M.T., Negri, S., Nuzzo, L., Quarta, T., Villani, A.V., 2000. A ground-penetrating radar survey for archaeological investigations in an urban area (Lecce, Italy). Journal of Applied Geophysics 44, 15–32.

Bertero, M., Boccacci, P., 1998. Introduction to Inverse Problems in Imaging. Institute of Physics Publishing, Bristol.

Colton, D., Kress, R., 1992. Inverse acoustic and electromagnetic scattering theory. Springer Verlag.

Conyers, L.B., Goodman, D., 1997. Ground-penetrating radar – An introduction for archaeologists. Alta Mira Press, Walnut Creek.

Cui, T.J., Chew, W.C., 2002. Diffraction tomographic algorithm for the detection of three-dimensional objects buried in a lossy half-space. IEEE Trans. Antennas Propagation 50, 42–49.

Daniels, D., 2004. Ground penetrating Radar, 2nd Ed. IEE Press, London. U.K.

Leckebusch, J., 2003. Ground-penetrating radar: a modern three-dimensional prospection method. Archaeological Prospection 10, 230–240.

Malagodi, S., Orlando, L., Piro, S., Rosso, F., 1996. Location of archaeological structures using GPR method. Three-Dimensional data acquisition and radar signal processing. Archaeological Prospecting 3, 13–23.

Meincke, P., 2001. Linear GPR inversion for lossy soil and a planar air-soil interface. IEEE Trans. on Geoscience and Remote Sensing 39, 2713–2721.

Martino, L., Bonomo, N., Lascano, E., Osella, A., Ratto, N., 2006. Electrical and GPR prospecting at Palo Blanco archaeological site, northwestern Argentina. Geophysics 71 (6), B193–B199.

Munro-Hay, S., 1991. Aksum, an African Civilization of Late Antiquity, (Dedicated to the late H. Neville Chittick). British Library Cataloguing in Publication Data.

Orlando, L., 2005. Joint interpretation of geophysical data for archaeology. A case study. Subsurface Sensing Technologies and Applications 6 (2), 235–250 Published online August 9, 2005.

Orlando, L., 2006. Environmental impact assessment for the re-erection of the returned stela to the Axum achaeological park (Ethiopia). 11th International Conference on Ground Penetrating Radar, June 19-22, 2006, Combus Ohio USA. CD-Rom.

Phillipson, D.W., 1991. Archaeology at Aksum, Ethiopia. Memories of the British Institute in Eastern Africa: number 17, report 65, research committee of the Society of Antiquaries of London.

Persico, R., Soldovieri, F., 2004. Reconstruction of a slab embedded in a three layered medium from multifrequency data under Born approximation. Journal of the Optical Society of America, Pt. A 21, 35–45.

Pierri, R., Brancaccio, A., Leone, G., Soldovieri, F., 2002. Electromagnetic prospection via homogeneous and inhomogeneous plane waves: the case of an embedded slab, AEÜ. International Journal of Electronics and Communications 56, 11–18.

Piro, S., Goodman, D., Nishimura, Y., 2002. The location of Emperor Traiano's villa altopiani di Arcinazzo-Roma) using high-resolution GPR surveys. Bollettino di Geofisica Teorica ed Applicata 43, 143–155.

Soldovieri, F., Persico, R., 2004. Reconstruction of an embedded slab from multifrequency scattered field under Born approximation, IEEE Trans. Antennas and Propagation 52, 2348–2356.

Soldovieri, F., Persico, R., Leone, G., 2005. Effect of source and receiver radiation characteristics in subsurface prospecting within the distorted Born approximation. Radio Science 40 (3) Art. No. RS3006.

Tallini, M., Giamberardino, A., Ranalli, D., Scozzafava, M., 2004. GPR survey for investigation in building foundations. Proceedings of GPR 2004, 10th International Conference on Ground Penetrating Radar, Delft, The Netherlands, pp. 395–397. Expanded Abstracts.

Yilmaz, Ö., 2001. Seismic data analysis. In: Doherty, S.M. (Ed.), Society of Exploration Geophysics.

Whiting, B.M., McFarland, D., Douglas, P., Hackenberger, S., 2000. Preliminary results of three-dimensional GPR-based study of a prehistoric site in Barbados, West Indies. SPIE Proceedings Series 4084, 260–267.